

PIV INVESTIGATION OF THE INTERNAL FLOW STRUCTURE IN A CENTRIFUGAL PUMP IMPELLER

N. Pedersen (np@et.dtu.dk)¹ and C.B. Jacobsen²

¹Dept. of Energy Engineering, Fluid Mechanics Section
Building 403, Technical University of Denmark
DK-2800 Lyngby, Denmark

²Fluid Dynamics Engineering
Grundfos A/S, DK-8500 Bjerringbro, Denmark

ABSTRACT

The internal flow structure in a centrifugal pump impeller is investigated using Particle Image Velocimetry (PIV). The measurements are performed in a perspex model of an industrial centrifugal impeller employing fluorescent seeding particles to give full access to near-wall flows. A large number of velocity vector maps are acquired by conditional sampling in a horizontal constant-height plane between hub and shroud of the impeller, with the 93*94 mm field-of-view in effect covering a full impeller passage. Instantaneous and ensemble averaged vector maps are transformed to the moving frame and analysed for the purpose of identifying steady and unsteady flow phenomena at different flow rates, with the main focus on severe off-design conditions.

At the nominal design point, the mean field of relative velocity is vane congruent in the predominant parts of the impeller passage, showing well-behaved flow with no separation. High levels of turbulence are confined to near-wall regions along the suction side. At the one-quarter load, results show every second blade passage being stalled while the adjacent blade passage performed well, as indicated in the instantaneous vector map shown in **Error! Unknown switch argument.** A large recirculation bubble formed on the suction side, in effect blocking most of the entrance to the stalled passage. Furthermore, a strong component of backflow was found at the pressure side near the impeller outlet. The detected stall phenomenon is stationary and non-rotating, and is not initiated via the interaction with any stationary components outside the impeller. In these respects, it differs from the phenomena commonly known as rotating stall.

The experimental setup and technique has proved to be efficient in providing reliable data over a full blade passage, also in the close vicinity of walls.

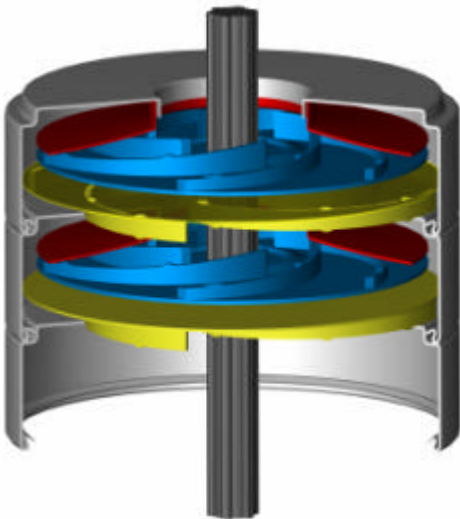


Figure **Error! Unknown switch argument.**: Multi-stage centrifugal pump showing the tested impeller geometry (Grundfos A/S).

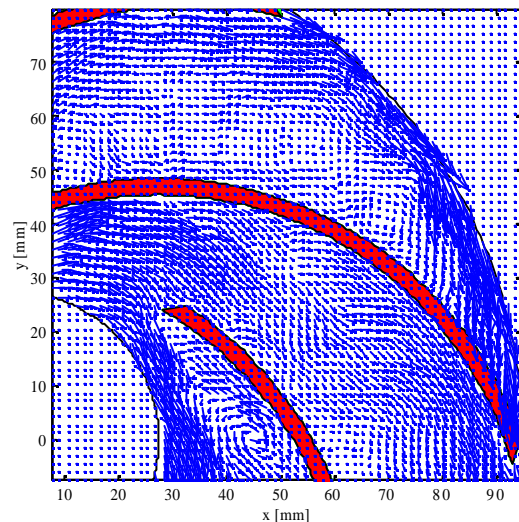


Figure **Error! Unknown switch argument.**: Sample instantaneous PIV vector map of the relative velocity \vec{w}

in the impeller at part-load conditions. $Q=0.25Q_n$

1. INTRODUCTION

Detailed knowledge of the flow field occurring inside impeller channels are important for further improvements in the design of centrifugal pumps. To this end, instantaneous data as given by PIV have proven a valuable supplement to mean data as a tool for the identification of unsteady and secondary flow phenomena. Several PIV studies have focused on the flow in the non-rotating components of a centrifugal pump stage. Akin and Rockwell (1994) used PIV to study the wake from a model impeller and its interaction with a stationary diffuser blade. They characterized flow separation and reattachment events using instantaneous streamline patterns and vorticity contours. Eisele et al. (1997) used PTV (Particle Tracking Velocimetry) in a vaned diffuser and found several unsteady flow features, i.e. a recirculating back flow from the diffuser into the impeller at part-load conditions. Other studies measured the flow in volutes, e.g. Dong et al. (1992a,b) who showed that the entire flow in the volute is pulsating, and that mean properties therefore cannot be used for estimating conditions near the exit from the impeller.

Fewer studies have been concerned with the internal flow in centrifugal impellers. Most rotor investigations have dealt with centrifugal compressors, e.g. Fowler (1968) and Eckardt (1976), who revealed the presence of a jet-wake structure at the discharge of the rotor. Measurements of the instantaneous internal flow in centrifugal pump impellers are scarce, and have only recently been reported done with PIV, see e.g. Oldenburg and Pap (1996) and Aramaki and Hayami (1999). Wernet (2000) provides an overview of the current state-of-the-art.

The objective of the present study is to investigate the flow inside the passages of a centrifugal pump impeller by PIV. The focus is on the use of instantaneous data to identify steady and unsteady flow phenomena at different operating conditions. Such data also serve to evaluate computational model studies such as Large Eddy Simulations.

2. EXPERIMENTAL SETUP

2.1 Impeller

The impeller under investigation was a medium specific speed shrouded impeller of industrial design, representing the rotor part of a multi-stage centrifugal pump, see Figure **Error! Unknown switch argument.**. The test impeller had a diameter of 190 mm and consisted of 6 simple curvature blades of constant thickness between a plane hub and a curved shroud plate. The axial height of the impeller passages was tapered from 13.8 mm at the inlet to 5.8 mm at the outlet. To facilitate optical measurements inside the impeller passages, the entire test impeller was manufactured in perspex which was subsequently polished on all internal and external surfaces. **Error! Unknown switch argument.** shows a plan view of the test impeller and the main dimensions are given in **Error! Unknown switch argument.**

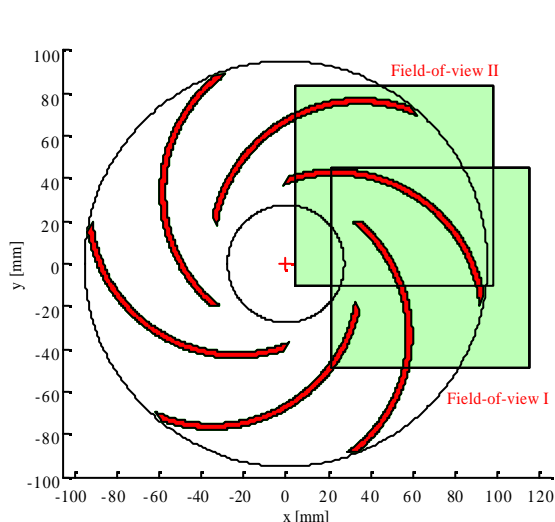


Figure **Error! Unknown switch argument.**: Plan view of the 190 mm diameter test impeller. The locations of the two 93*94 mm fields-of-view measured with PIV

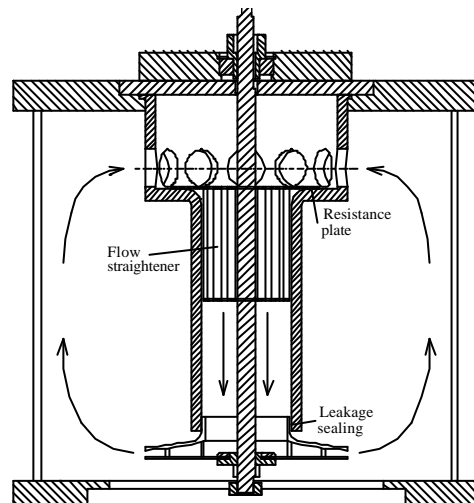


Figure **Error! Unknown switch argument.**: Closed-loop test-rig with optical access provided from the sides as well as from beneath.

are shown.

Table Error! Unknown switch argument.: Impeller geometry

Inlet diameter	D_1	77	[mm]
Outlet diameter	D_2	190	[mm]
Inlet height	h_1	13.8	[mm]
Outlet height	h_2	5.8	[mm]
Number of blades	z	6	[-]
Blade thickness	t	3	[mm]
Inlet blade angle	β_1	19.7	[°]
Outlet blade angle	β_2	18.4	[°]

Table Error! Unknown switch argument.: Operating conditions

Rotational speed	n	725	[rpm]
Reynolds number	Re_D	$1.4 \cdot 10^6$	[-]
Specific speed	N_q	26.3	[eng]
Design flow rate	Q_n	3.05	[l/s]
Series I	$Q=Q_n$	3.05	[l/s]
Series II	$Q=0.25Q_n$	0.76	[l/s]

2.2 Test rig

As the purpose of the present study is to reveal phenomenological flow structures inside the impeller passages, rather than to predict the performance of a true pump stage, the experiments were done in a closed-loop test rig specially designed to provide easy optical access, see **Error! Unknown switch argument.**

The test rig was a 350 mm high, 400 mm diameter cylindrical tank with perspex casing and stainless steel top and bottom plates. The tank holds 40 liter of the working fluid, demineralised water. The impeller was mounted on a 16 mm diameter shaft placed vertically in the tank. A 220 mm long, 84 mm diameter straight perspex pipe was used as inlet to the impeller which discharged directly into the outer annulus of the cylindrical tank, where the water rose and recirculated into the central inlet pipe, see **Error! Unknown switch argument.** The flow rate through the impeller was adjusted by letting the fluid pass through a resistance plate with an array of small circular holes mounted in the top of the inlet pipe. By varying the diameter of the holes from 1 to 5 mm this allowed the intake area/system pressure drop to be varied to achieve flow rates in the range 15-100% of the nominal value Q_n . A flow straightener consisting of twelve 7 mm diameter pipes was mounted in the inlet pipe in order to eliminate fluctuations from the flow and maintain stable, well-defined inlet conditions to the impeller. Furthermore, a leakage sealing was installed to prevent fluid from entering the inlet pipe by flowing over the shroud plate. This effectively reduced the leakage flow, which was measured to attain a maximum value of 10% of nominal flow at shut-off conditions.

The cylindrical tank constitutes a simple closed-loop test rig with optical access provided in all horizontal planes, as well as from beneath via a 260 mm diameter glass plate mounted in the bottom plate. The impeller was driven by a frequency-controlled 0.37 kW motor enabling continuously variable speed control in the range 250-900 rpm. The measurements presented in this paper are all obtained at a constant rotational speed of 725 rpm at two different flow rates. The first series (I) is obtained at the nominal operating point, $Q_n=3.05$ l/s, and the second series (II) at part-load, $Q=0.25Q_n$. **Error! Unknown switch argument.** summarizes the operating conditions for the impeller.

2.3 PIV setup

Digital Particle Image Velocimetry measurements were performed inside the impeller in a horizontal x,y-plane positioned 2.9 mm above the plane hub, i.e. at mid passage-height at the impeller outlet. The light source was a double-cavity 532 nm Nd:YAG laser running at 10 Hz and with a pulse duration of 4-6 ns. An articulated light arm was used to direct the pulsing laser beams to the testrig where cylindrical optics produced a light sheet with a thickness of approximately 1.5 mm and a divergence angle of 15°. Fluorescent RhodaminB particles of spherical shape and with a mean diameter of $d_p=30$ μ m were used as seeding. Particle images were captured by a 1K x 1K cross-correlation CCD camera placed below the testrig at right angles to the laser-sheet, and looking at the illuminated seeding particles inside the impeller passages through the transparent hub plate. The camera was equipped with a 60 mm lens and a 550 nm optical cut-off filter which only transmitted the signal fluorescence wavelength and thus prevented flare light from the impeller blades from reaching the CCD sensor. The camera was mounted on a stepper-motor controlled three-axis traverse bench to ease positioning.

A once-per-revolution signal was obtained from the rotor shaft via a laser diode sensor system and was used to trigger the PIV acquisition. This allowed a large number of instantaneous samples to be obtained at the same

circumferential position of the impeller in order to calculate ensemble averages. **Error! Unknown switch argument.** shows the locations of the two 93 x 94 mm fields-of-view which was measured, in effect covering a full impeller passage. The corresponding magnification factor was $M=0.098$.

2.4 Data acquisition and processing

Care was taken to optimize the quality of the PIV data, both at the recording and at the processing stage. The entire cylindrical tank was flooded with particles to give a uniform and sufficiently high seeding concentration to ensure a minimum of 5-10 particles in each interrogation region. In order to minimize the displacement estimation error, the numerical aperture of the recording lens was chosen so diffracted particle images covered at least 1-2 pixels on the CCD sensor (Westerweel 1998). Based on M and the particle diameter d_p , this requirement imposed an f-number of $f\# = 8$. The pulse delay Δt was set as according to the $\frac{1}{4}$ displacement rule (Keane and Adrian 1990) to 150 and 110 μs for series I and II, respectively.

The conditionally sampled PIV images were processed into vector maps using the cross-correlation method and interrogation areas of 32 by 32 pixels and 50% overlap. This yielded 60 x 60 vectors per vector map with a distance of 1.5 mm between each vector. Due to the use of high-density fluorescent seeding a good signal-to-noise ratio were obtained even in the close proximity of the impeller blades. Therefore the number of spurious vectors (outliers) did not exceed 1-3% which is significantly lower than if non-fluorescent seeding were used. Subsequently, the only validation procedure applied was a removal of vectors with a correlation peak signal-to-noise ratio below 1.20. No interpolation or data filling was applied.

Experimental uncertainties include variations in the impeller speed, estimated to $\pm 1.5\%$, and an uncertainty of $\pm 3\%$ in the flow rate specification. The errors inherent to the instantaneous PIV velocity estimates themselves are estimated to be of the order of 1% (Westerweel 1997). Sample sizes of 2000 vector maps were collected to ensure an accuracy of 0.7% and 4.5% (c.i. = 95%) on the mean and fluctuating components of velocity, respectively. The total recording time of 2000 conditionally sampled images was in the order of 0.6h, which corresponds to a mean acquisition rate of 0.8 Hz.

3. RESULTS AND DISCUSSION

Error! Unknown switch argument. shows a sample of the particle images acquired in the impeller in field-of-view II (see Figure **Error! Unknown switch argument.**). The rotation sense is anti-clockwise and the laser-sheet direction is from upper right to lower left as indicated by the weak shadow behind the trailing edge of the vane in the top of the image. **Error! Unknown switch argument.** shows a sample instantaneous vector map of the absolute velocity \vec{c} , which is readily obtained in the fixed camera reference frame. The flare of the assembly screws visible in Figure **Error! Unknown switch argument.** was used for referencing.

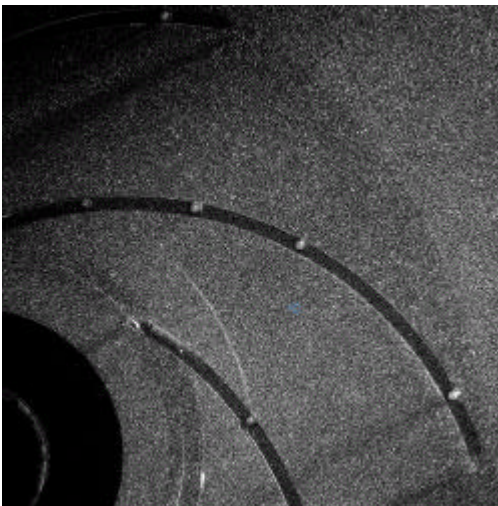


Figure **Error! Unknown switch argument.**: Sample particle image of the impeller. The rotation sense is anti-clockwise. The laser sheet direction is from upper

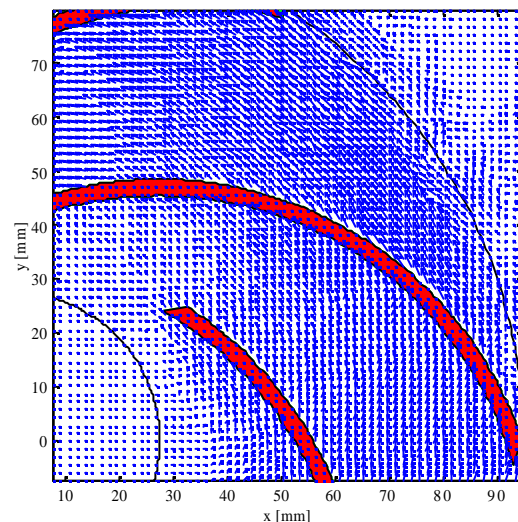


Figure **Error! Unknown switch argument.**: Sample instantaneous velocity vector map of the absolute velocity \vec{c} . Corresponding relative velocity vector map

right to lower left.

is shown in **Error! Unknown switch argument.**.
 $Q=0.25Q_n$

In order to interpret the flow structures inside the impeller passages, the velocity \bar{w} relative to the rotating impeller was calculated. This is given by $\bar{w} = \bar{c} - \bar{u}$, i.e. by vectorial subtraction of the local circumferential impeller speed from the measured data. Figure **Error! Unknown switch argument.** shows the instantaneous relative velocity corresponding to the absolute vector map in Figure **Error! Unknown switch argument.**.

3.1 Full-load

Figure **Error! Unknown switch argument.** shows the ensemble average of 2000 instantaneous realizations acquired at the nominal flow rate Q_n in field-of-view I (see Figure **Error! Unknown switch argument.**). It is seen that the mean field of relative velocity is close to vane congruent in the predominant parts of the impeller passage. The flow increases along the suction side without separation due to the low dynamic loading at this operating point. Only a careful investigation of the results indicate that the sharp leading edge of the impeller vanes slightly perturbs the flow on the blade pressure side.

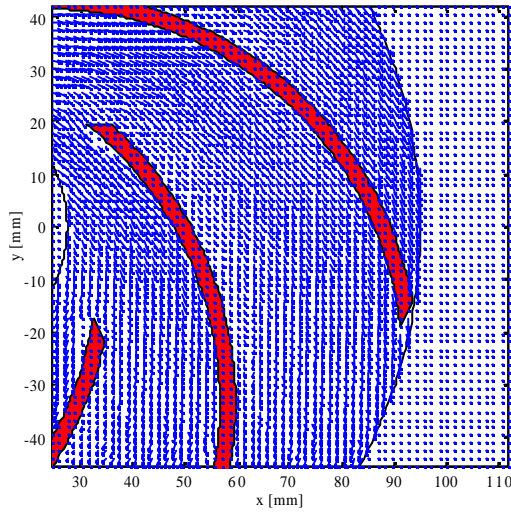


Figure **Error! Unknown switch argument.**: Ensemble average of 2000 instantaneous PIV vector maps. $Q=Q_n$

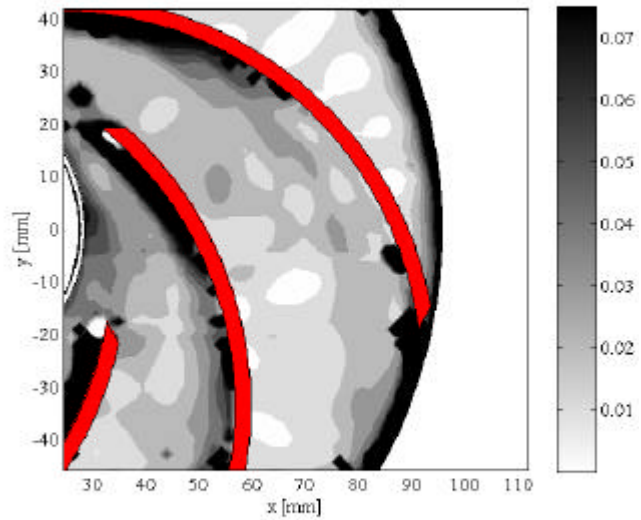


Figure **Error! Unknown switch argument.**: Contour plot of the measured portion k_{2D} of the turbulent kinetic energy. $Q=Q_n$

A quantitative measure of the extent of random unsteady velocity fluctuations is the measured portion k_{2D} of the turbulent kinetic energy k , defined as the mean deviation of instantaneous data from the ensemble-averaged results

$$k_{2D} = \frac{1}{2} \left(\langle c_x'^2 \rangle + \langle c_y'^2 \rangle \right) \quad (1)$$

where ' denote a velocity fluctuation, $\langle \rangle$ an ensemble average, and c_x and c_y are the planar absolute velocity components. It is noted that this quantity does not account for the span-wise velocity fluctuations, not measured. A contour plot of k_{2D} is given in Figure **Error! Unknown switch argument.** and demonstrates an even distribution of turbulent kinetic energy, with higher levels of turbulence confined to near-wall areas along the vane suction side. Based on k_{2D} , a turbulence intensity may be defined as $Tu = \sqrt{k_{2D}} / U_2$ where U_2 is the impeller speed at the outlet. Values of turbulence intensity reach a maximum of 4% at the suction side, but are otherwise much lower confirming the persistence of an inviscid potential flow core in the impeller passage at full-load conditions.

3.2 Part-load

The main focus of the present work was to investigate the flow characteristics of the centrifugal impeller operating at severe off-design conditions. Figure **Error! Unknown switch argument.** shows a snapshot of the flow measured in field-of-view II at a flow rate of $0.25Q_n$. The ensemble average based on 2000 vector maps is presented in Figure

Error! Unknown switch argument. Both vector maps show a clear departure from the well-behaved, non-separated flow field present at full-load. A large recirculation bubble has formed at the suction side of the vane in the lower part of the field-of-view. Furthermore, a low-velocity zone with an array of counter-rotating vortices has emerged in the upper passage, extending over half the passage-width on almost the entire pressure side. A strong component of backflow into the upper passage is also seen on the ensemble average, reducing the through-flow in this passage. In contrast, the center passage shows no evidence of separated flow, but is fairly well-behaved, although exhibiting fluctuations in the relative flow angle along the passage.

In order to highlight instantaneous flow structures, the deviation of a sample instantaneous velocity \vec{c} from the ensemble average $\langle \vec{c} \rangle$ is shown in Figure **Error! Unknown switch argument.**. This gives evidence of a highly fluctuating flow. Note that these fluctuating velocities also represent those of the relative field, i.e. $\vec{w} - \langle \vec{w} \rangle$.

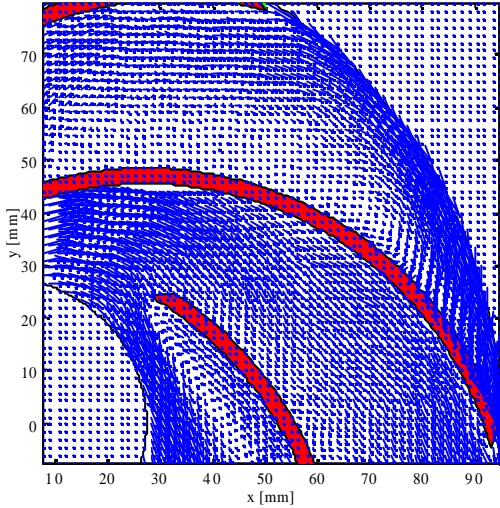


Figure **Error! Unknown switch argument.**: Ensemble average of 2000 instantaneous PIV vector maps. $Q=0.25Q_n$

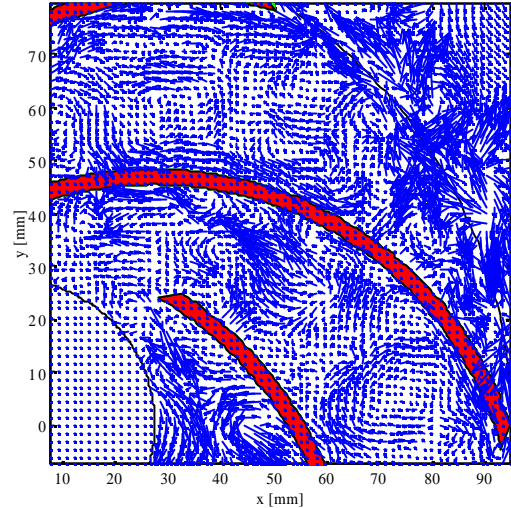


Figure **Error! Unknown switch argument.**: Sample instantaneous deviation $\vec{c} - \langle \vec{c} \rangle$ from the ensemble average. $Q=0.25Q_n$

The fact that adjacent impeller passages exhibit such distinct flow characteristics suggests that every second impeller passage is stalled at quarter-load. To explore this further, a supplementary series of PIV data were acquired with the camera in the same location, but with an additional delay of $T/6=13.8$ ms, i.e. the passage time of one impeller blade, added to the trigger signal from the rotor shaft. Because of the stationary appearance of the detected stall phenomena, this allowed us to collect data in a region that effectively covered two full adjacent passages. Following this procedure, another 2000 samples were collected. The results are shown in Figure **Error! Unknown switch argument.**. The last series, although acquired at the same location, has been rotated 60 degrees to reflect the effective field-of-view.

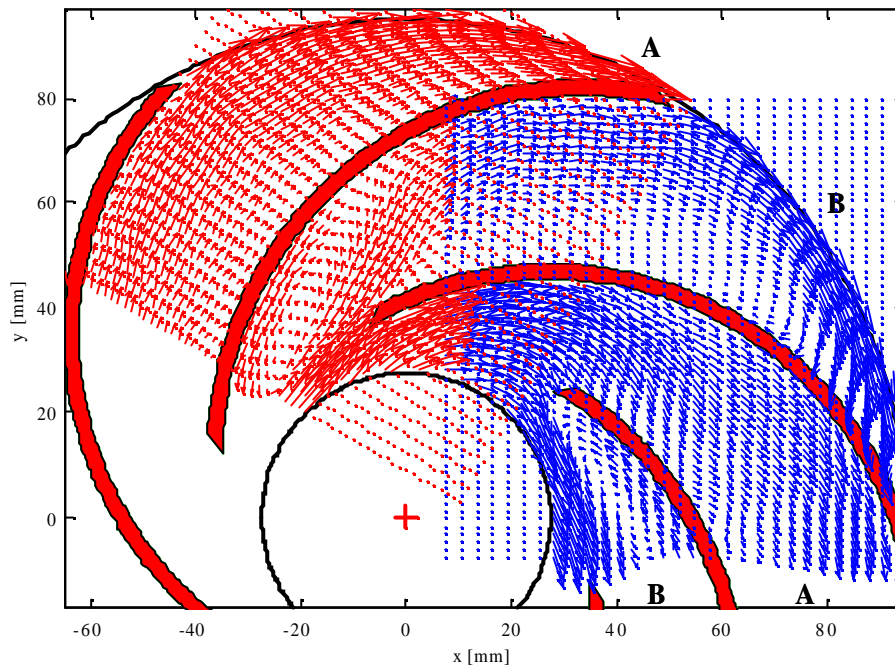


Figure Error! Unknown switch argument.: Two ensemble averages of each 2000 vector maps acquired separately. One set of data has been rotated 60 degrees to facilitate comparison. Only every second vector is shown to avoid crowding. The well-behaved passage is denoted A and the stalled one B. $Q=0.25Q_n$

It is apparent from Figure **Error! Unknown switch argument.** that the two different ensemble averages fit perfectly together and therefore fully correspond with the result obtained had the two series been acquired simultaneously. For the aid of discussion, the impeller passage without flow separation has been denoted A and the stalled one B. The large extent of the suction side recirculation zone in passage B is notable, with flow reattaching not taking place until half-way down the blade. The recirculation bubble effectively blocks three-quarters of the entrance to passage B, which in return gives rise to the low-velocity zone inside the passage, and furthermore apparently unstalls passage A.

A contour plot of the turbulent kinetic energy measured at $Q=0.25Q_n$ is given in Figure 12. The contours show a highly elevated level of k_{2D} in a region extending from the leading edge along the core of the suction side separation bubble towards the leading edge of the next arriving impeller vane. High levels of turbulence also exist on the pressure side near the outlet of passage B, coinciding with the location of strong backflow. Generally, k_{2D} attains values more than twice the level measured at full-load conditions. Expressed in terms of Tu , local values as high as 10% are found in the regions described. In addition to this, it should be noted that if referred to local relative velocities instead of the outlet wheel speed U_2 , the turbulence intensities could be even higher.

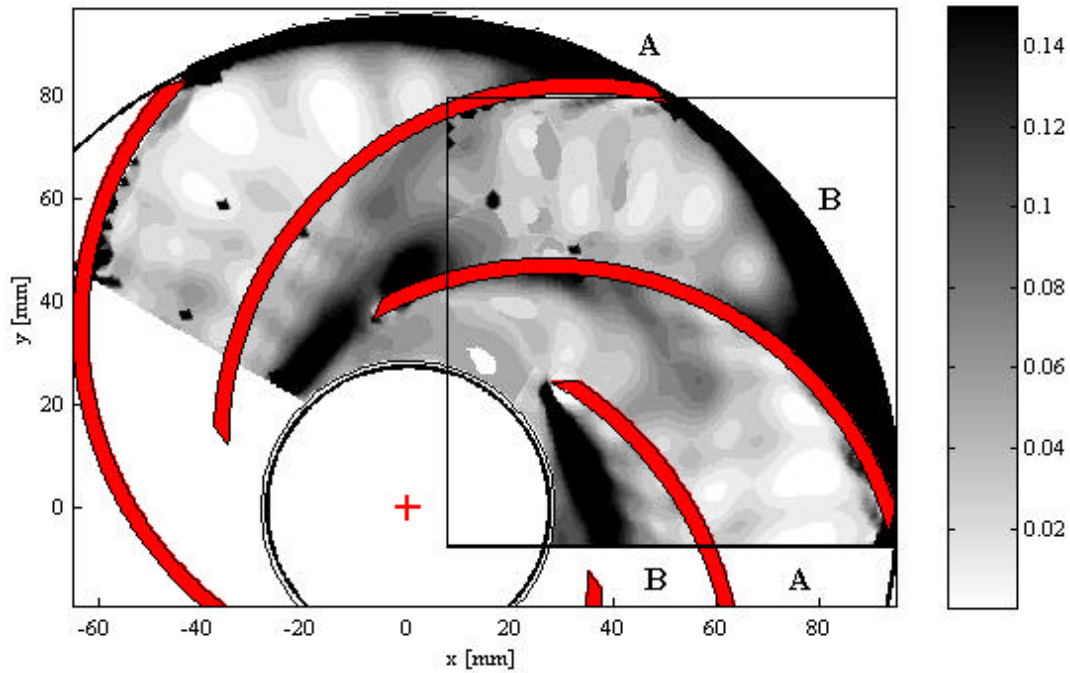


Figure **Error! Unknown switch argument.**: Contour plot of the measured portion k_{2D} of the turbulent kinetic energy. One set of data has been rotated 60 degrees to facilitate comparison. The well-behaved passage is denoted A and the stalled one B. $Q=0.25Q_n$

3.3 Radial velocity

The blade-to-blade distributions of the ensemble-averaged radial velocity component w_r have been extracted from the PIV data and are shown in Figure **Error! Unknown switch argument.** for the flow rates of Q_n and $Q=0.25Q_n$. The velocity profiles are made dimensionless with the wheel speed at the outlet U_2 , and are given for radii of $r = 0.50R_2$, $0.75R_2$ and $r = 0.98R_2$ (impeller outlet), respectively.

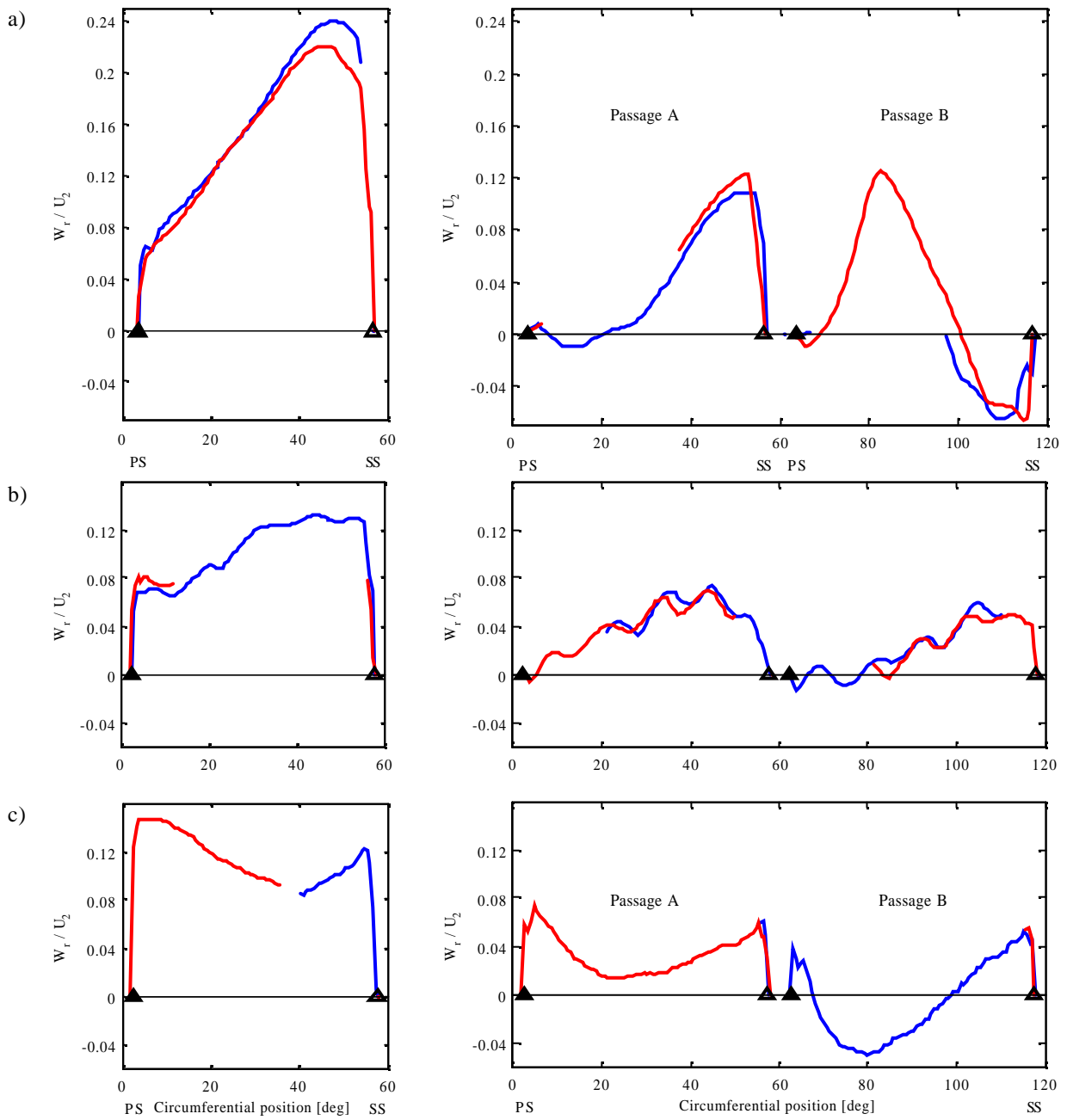


Figure Error! Unknown switch argument.: Blade-to-blade distribution of the ensemble-averaged normalized radial velocity component w_r , measured with PIV at flow rates of $Q=Q_n$ (left) and $Q=0.25Q_n$ (right). a) $r=0.50R_2$ b) $r=0.75R_2$ c) $r=0.98R_2$.

The left column of Figure 13 shows the results for full-load, and the right column for quarter-load. The latter shows two pressure-to-suction side intervals in order to represent the unstalled and stalled passages A and B, respectively. All graphs show one or two lines on top of each other depending on the available data at the individual radial station, demonstrating the high degree of reproducibility of the measurements.

At full-load, the profile at $r=0.50R_2$ is shifted markedly towards the suction side (SS), indicating a somewhat prerotated inlet flow. Travelling outwards through the impeller passage the radial velocity profile evens out, and at the outlet the highest velocity has shifted to the pressure side (PS). This pattern is in accordance with classical streamline theory.

Moving on to the quarter-load data, passage A exhibits the same main features as seen at full-load, with the addition of local flow features such as backflow at the inner radial station. In contrast, the inlet profile of passage B is shifted towards the pressure side with backflow velocities at the suction side reaching a magnitude of 55% of the maximum outward component. In both passages a persistent wavy profile is seen at the $r=0.75R_2$ station. This is also visible on the vector map in Figure 11. The outer radial station of channel B gives evidence of a stalled passage with almost no through-flow. Comparing the inner and outer radial stations of channel B suggests that three-dimensional effects are present in this industrial-type impeller. To elaborate further on this, LDA data obtained at the same operating conditions, but at different axial positions, are presently being analysed.

4. CONCLUSIONS

Detailed particle image velocimetry measurements using fluorescent seeding have been performed inside the passages of a perspex centrifugal impeller of industrial design. The main focus of the investigation has been to study steady and unsteady flow features at severe off-design conditions. The experimental setup and technique has proved to be efficient in providing reliable data over a full blade passage, also in the close vicinity of walls.

Measurements performed at the nominal operating point Q_n show a well-behaved vane congruent flow with no separation occurring. At part-load at a flow rate of $Q=0.25Q_n$ stall is detected in every second passage, while the adjacent passages are unstalled and exhibit well-behaved flow. High levels of turbulence are found in the stalled passage in a strong separation bubble at the suction side at inlet, and at the pressure side at outlet.

The stall phenomenon detected is stationary and non-rotating. This may be due to the even number of vanes and the fact that the stall is not initiated via the interaction with any stationary components outside the impeller. In these respects, the present stall phenomenon differs from the periodic unsteadiness of the relative flow commonly known as rotating stall, which typically moves in the direction of rotation at a lower speed than the impeller.

ACKNOWLEDGEMENTS

The study was partially supported by grants from Grundfos A/S, Bjerringbro, Denmark and Technical University of Denmark.

REFERENCES

- O. Akin and D. Rockwell (1994). Flow structure in a radial flow pumping system using high-image-density Particle Image Velocimetry. *J. Fluids Engng.*, **116**, 538-544.
- S. Aramaki and H. Hayami (1999). Unsteady flow measurement in a rotating impeller using PIV. In Proceedings of the 3rd International Workshop on PIV, Santa Barbara, California, USA, 16-18 September.
- R. Dong, S. Chu, and J. Katz (1992a). Quantitative visualization of the flow within the volute of a centrifugal pump. Part A: Technique. *J. Fluids Engng.*, **114**, 390-395.
- R. Dong, S. Chu, and J. Katz (1992b). Quantitative visualization of the flow within the volute of a centrifugal pump. Part B: Results and analysis. *J. Fluids Engng.*, **114**, 396-403.
- D. Eckardt (1976). Detailed flow investigations within a high-speed centrifugal compressor impeller. *J. Fluids Engng.*, 390-402, 1976.
- K. Eisele, Z. Zhang, and M. Casey (1997). Flow analysis in a pump diffuser - Part 1: LDA and PTV measurements of the unsteady flow. *J. of Turbomachinery*, **119**, 968-977.
- H. Fowler (1968). The distribution and stability of flow in a rotating channel. *J. Eng. Power*, 229-236.
- R.D. Keane and R.J. Adrian (1999). Optimization of particle image velocimeters. Part I: Double pulsed systems. *Meas. Sci. Technology*, **1**, 1202-1215.

M. Oldenburg and E. Pap (1996). Velocity measurements in the impeller and in the volute of a centrifugal pump by Particle Image Displacement Velocimetry. Proceedings of the 8th International Symposium on Applications of Laser Techniques to Fluid Mechanics, pages 8.2.1-8.2.5.

M.P. Wernet (2000). Development of digital particle imaging velocimetry for use in turbomachinery. *Exp. Fluids*, **28**, 97-115.

J. Westerweel (1997). Fundamentals of digital particle image velocimetry. *Meas. Sci. Technology*, **8**, 1379-1392.

J. Westerweel (1998). Effect of sensor geometry on the performance of PIV interrogation. Proceedings of the 9th International Symposium on Applications of Laser Techniques to Fluid Mechanics, pages 1.2.1-1.2.8.